# Supplementary Material

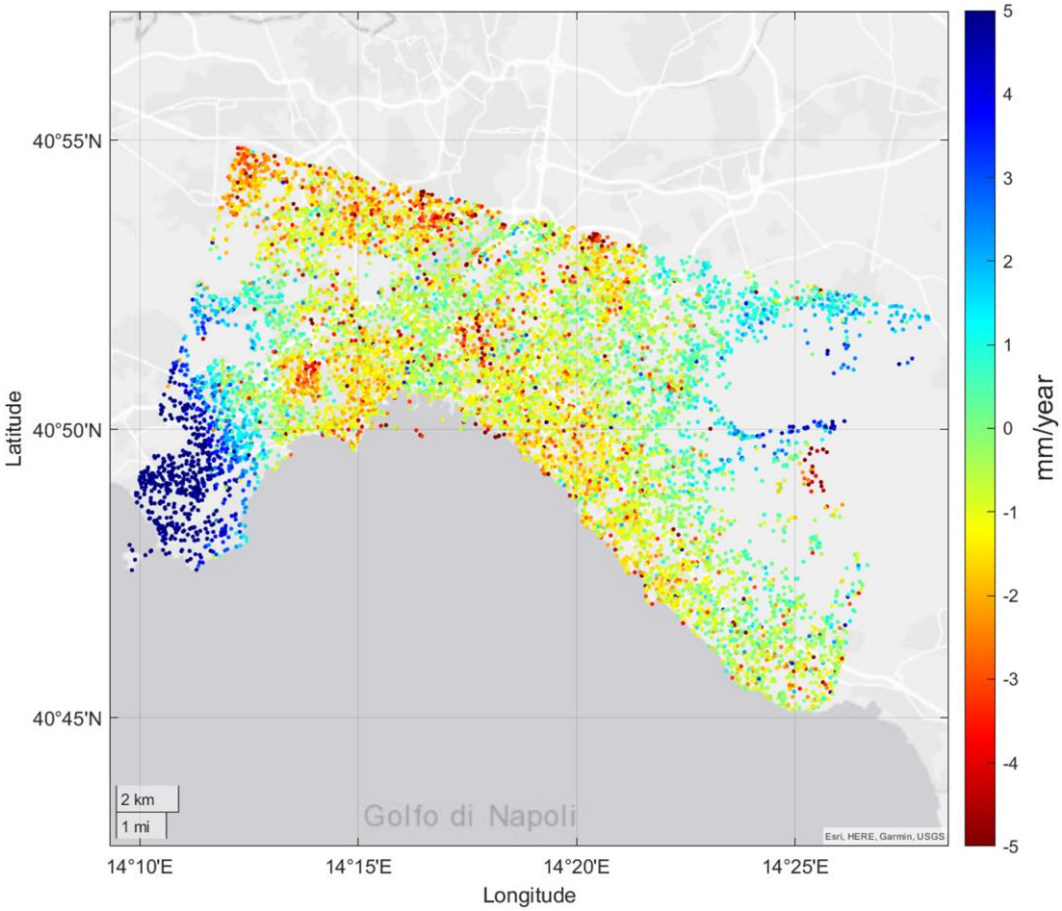


**Figure S1.** Mean LOS velocity map from the TerraSAR-X dataset.

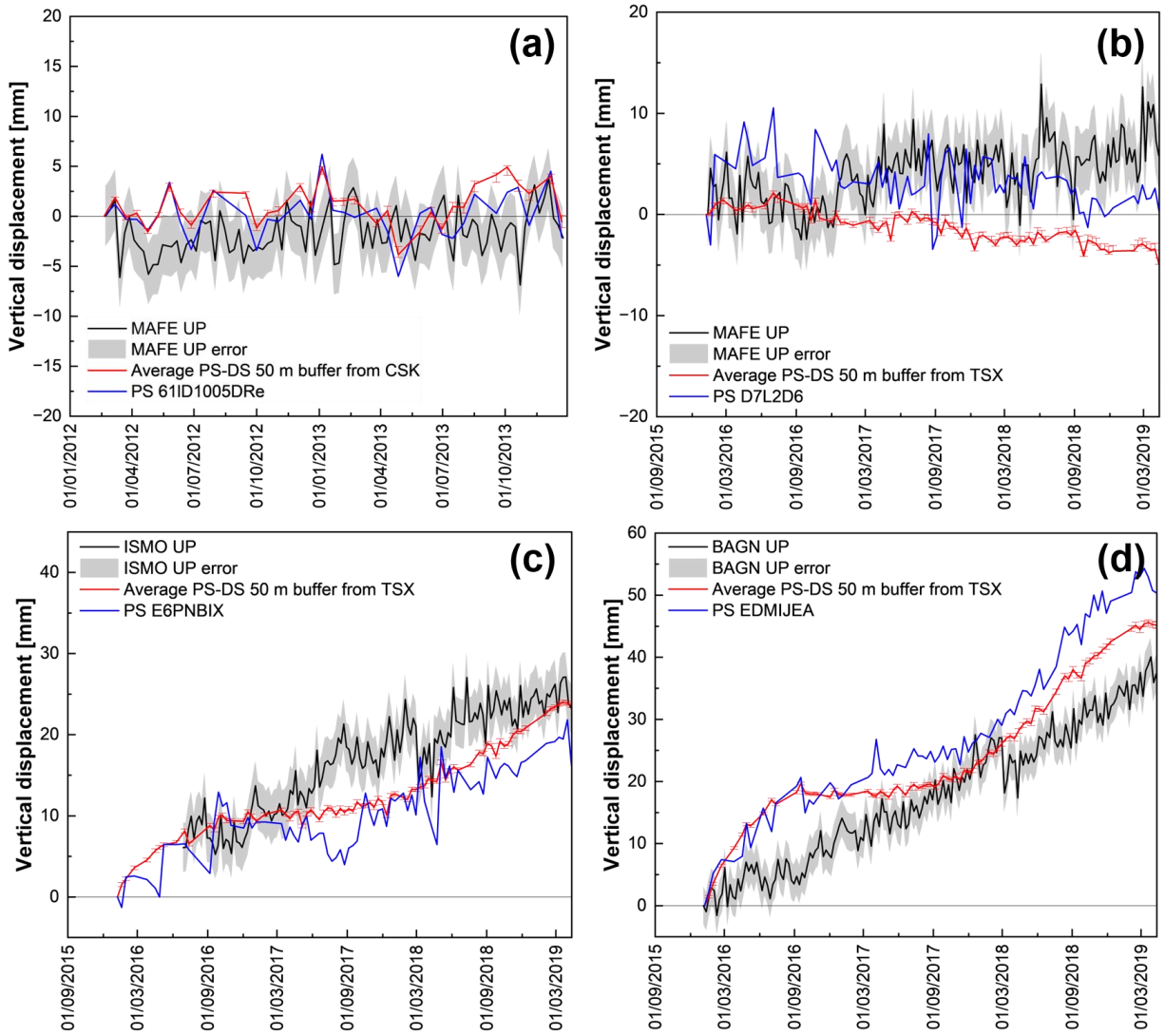


**Figure S2.** (a) Comparison of CSK and cGPS MAFE measurements; (b–d) comparisons of TerraSAR-X with cGPS MAFE, cGPS ISMO and cGPS BAGN, respectively, in which the time intervals refer to the datasets. In every figure: grey shadow areas show the cGPS error measurements; red lines represent the average vertical displacements of PS-DSs at a buffer of 50 m from the cGPS stations; blue lines represent vertical displacements of the PSs closest to each cGPS station.

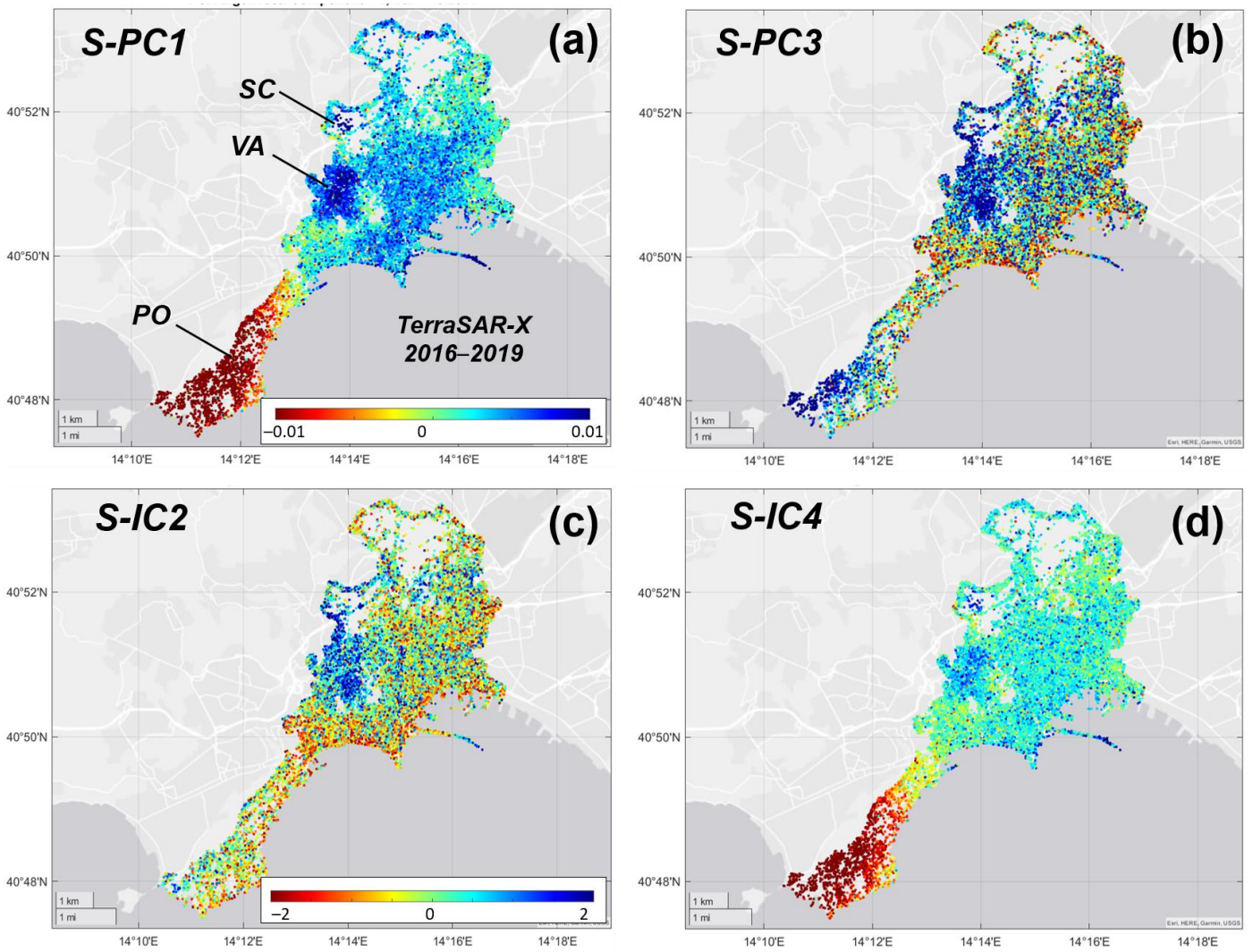


**Figure S3.** Spatial distributions of the components extracted from S-PCA and S-ICA on 20,000 randomly selected PS-DSs from TerraSAR-X within the UNESCO site. (a) S-PC1, (b) S-PC3, (c) S-IC2 and, (d) S-IC4.

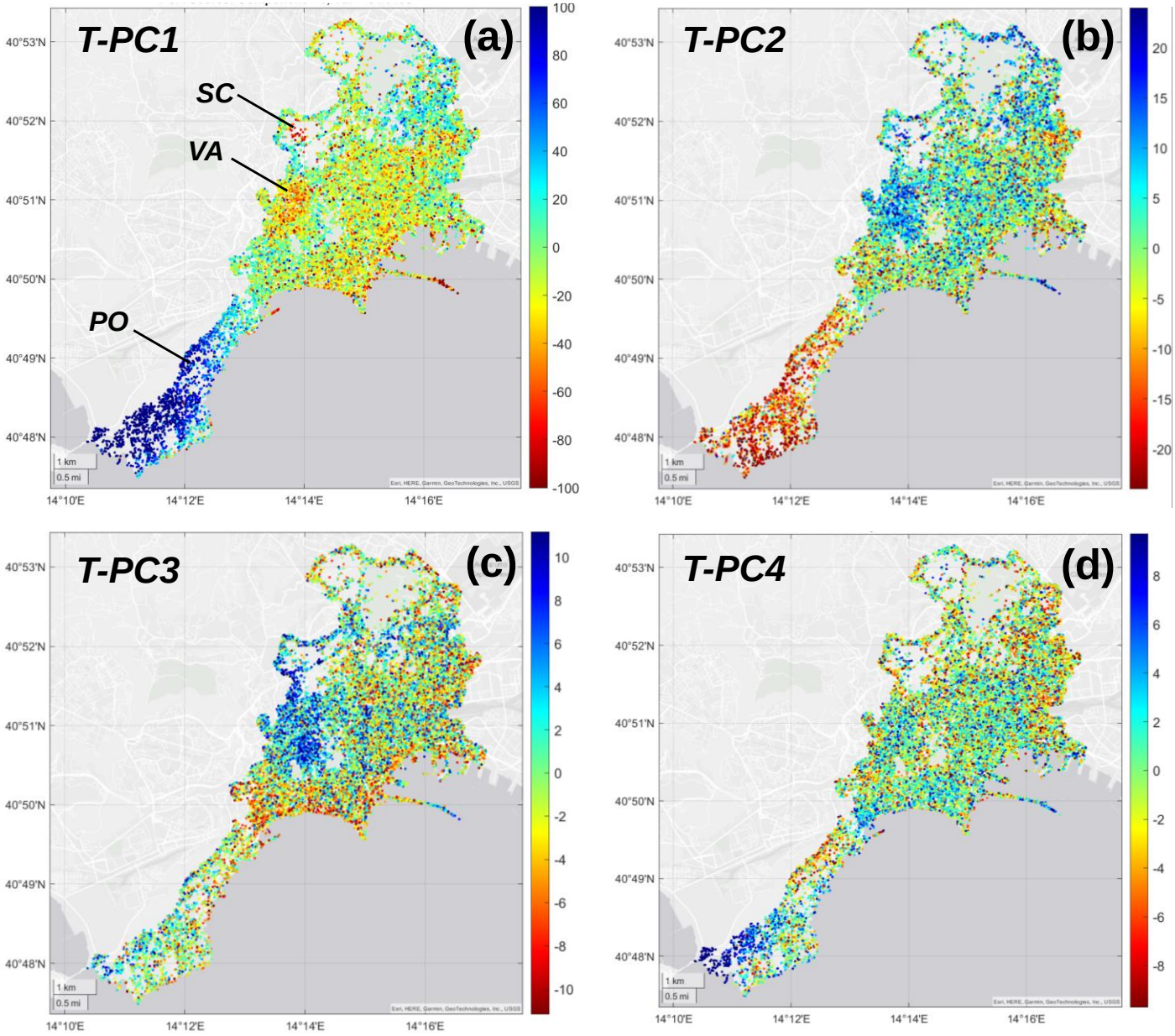


**Figure S4.** Spatial distributions of the components extracted from T-PCA on 20,000 randomly selected PS-DSs from TerraSAR-X within the UNESCO site. (a) T-PC1, (b) T-PC2, (c) T-PC3 and, (d) T-PC4.

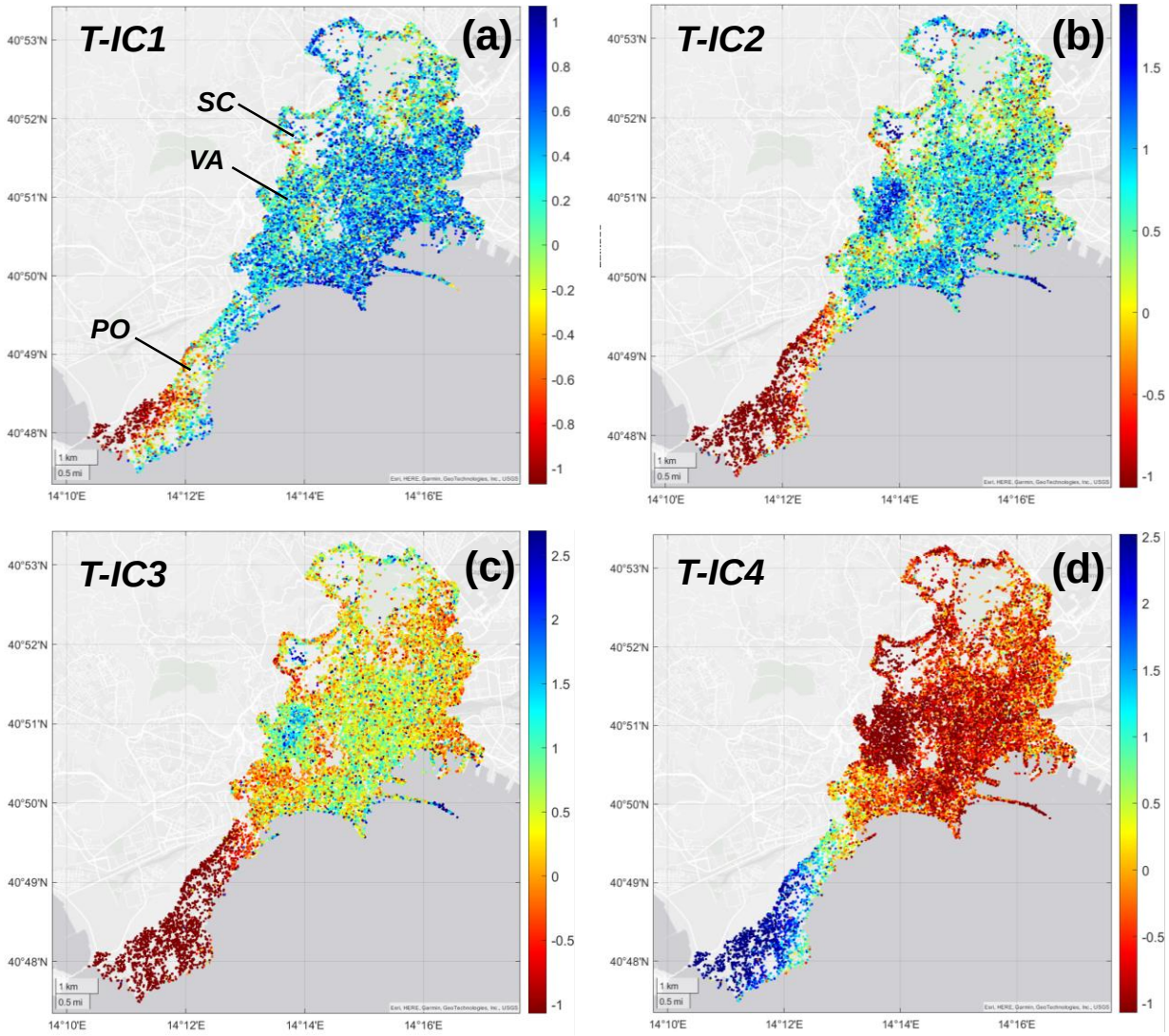


**Figure S5.** Spatial distributions of the components extracted from the T-ICA applied to 20,000 randomly selected PS-DSs from TerraSAR-X within the UNESCO site: (a) T-IC1, (b) T-IC2, (c) T-IC3 and, (d) T-IC4.

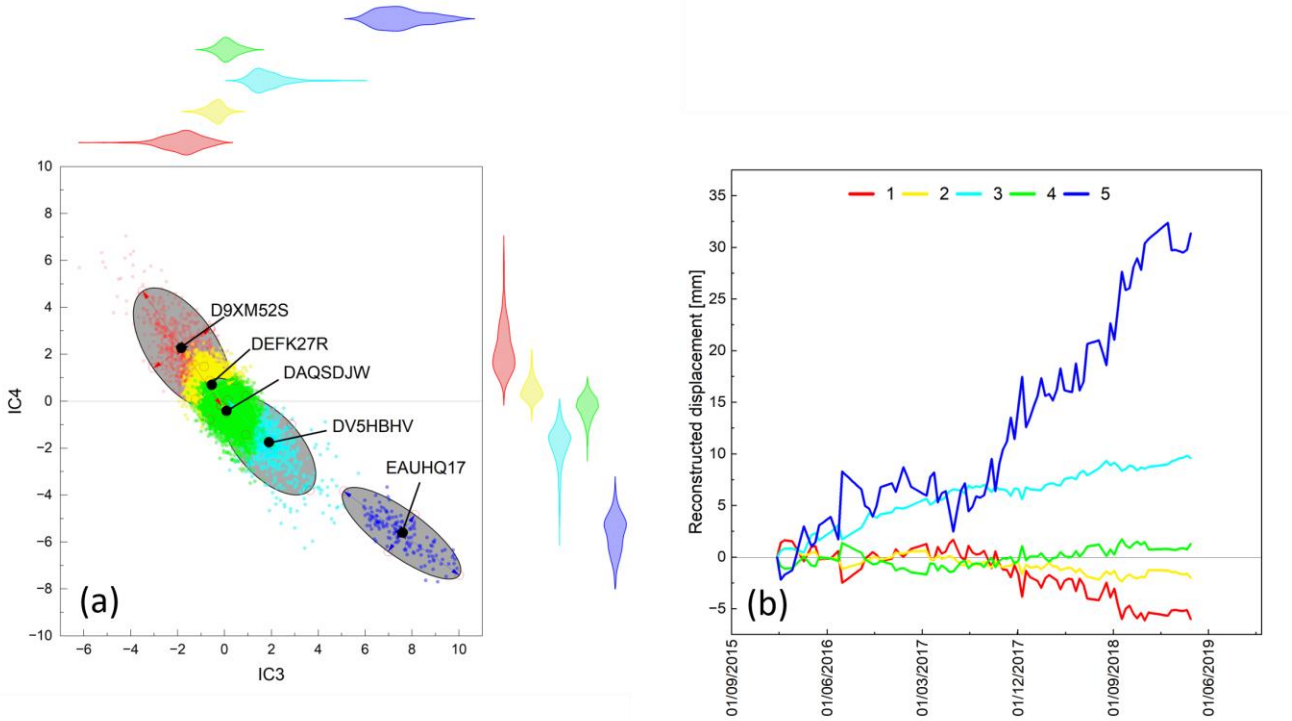


**Figure S6.** (a) IC3-IC4 plane projection of the five clusters obtained from T-ICA applied to TerraSAR-X PS-DSs above the 10 m buffers of the cavity's polygons. (b) Reconstructed time series of the five cluster centroids based on the four considered independent components.

**Table S1.** Table reporting the parameters characterizing five clusters obtained from the HC on the T-ICA analysis performed on the PS-DSs within the $20m$ buffer around each cavity. The table also reports the parameters characterizing the ellipse related to each cluster.

| | | Cluster Parameters | | | | | | Ellipse Parameter 95% | | | |
|---|---|---|---|---|---|---|---|---|---|---|---|
| **Cluster ID** | **N** | **Min IC3** | **Min IC4** | **Max IC3** | **Max IC4** | **SD IC3** | **SD IC4** | **a** | **b** | **IC3** | **IC4** |
| 1 | 734 | −6.19 | 0.16 | 0.13 | 7.04 | 0.84 | 1.05 | 2.96 | 1.48 | −1.81 | 2.25 |
| 2 | 7850 | −2.01 | −1.11 | 1.13 | 2.49 | 0.39 | 0.44 | 1.10 | 0.93 | −0.39 | 0.48 |
| 3 | 936 | 0.23 | −6.26 | 6.01 | −0.22 | 0.82 | 0.86 | 2.60 | 1.32 | 1.89 | −1.88 |
| 4 | 10,335 | −1.56 | −3.49 | 2.09 | 1.14 | 0.44 | 0.51 | 1.38 | 0.93 | 0.15 | −0.28 |
| 5 | 145 | 5.94 | −7.69 | 9.92 | −3.65 | 1.02 | 0.78 | 3.05 | 0.97 | 7.55 | −5.62 |

**Sinkholes Analysis**

Based on the recent inventory of "anthropogenic" sinkholes in the city of Naples [26], we compared the location of sinkholes with the cavity inventory [42,69]. Among the total 213 sinkholes, 20 are located within a 20 m buffer area surrounding each cavity. When increasing the buffer size from 20 to 30 m, twenty-two sinkholes were identified in the cavity surroundings (Figure S7). This outcome suggests that sinkholes located at a distance greater than 30 m from cavities may not be related to their presence. Furthermore, according to the results obtained by T-ICA performed on the PS-DSs located within the different buffer sizes (from 10 m to 50 m, see Figure 14b), when increasing the distance from the cavity, the subsidence effect markedly decreases and the dispersion of the data increases (as shown in Figure 14e,f), particularly starting from 20 m from the cavity.

Subsequently, we associated each selected sinkhole located within the buffer size of 30 m with the nearby cavity and considered only the eight sinkholes that occurred during the period monitored by TerraSAR-X (2015 − 2019). Among them, it was observed that 50% are related to cavities classified as cluster ID 2, and therefore characterized by less pronounced subsidence kinematics.

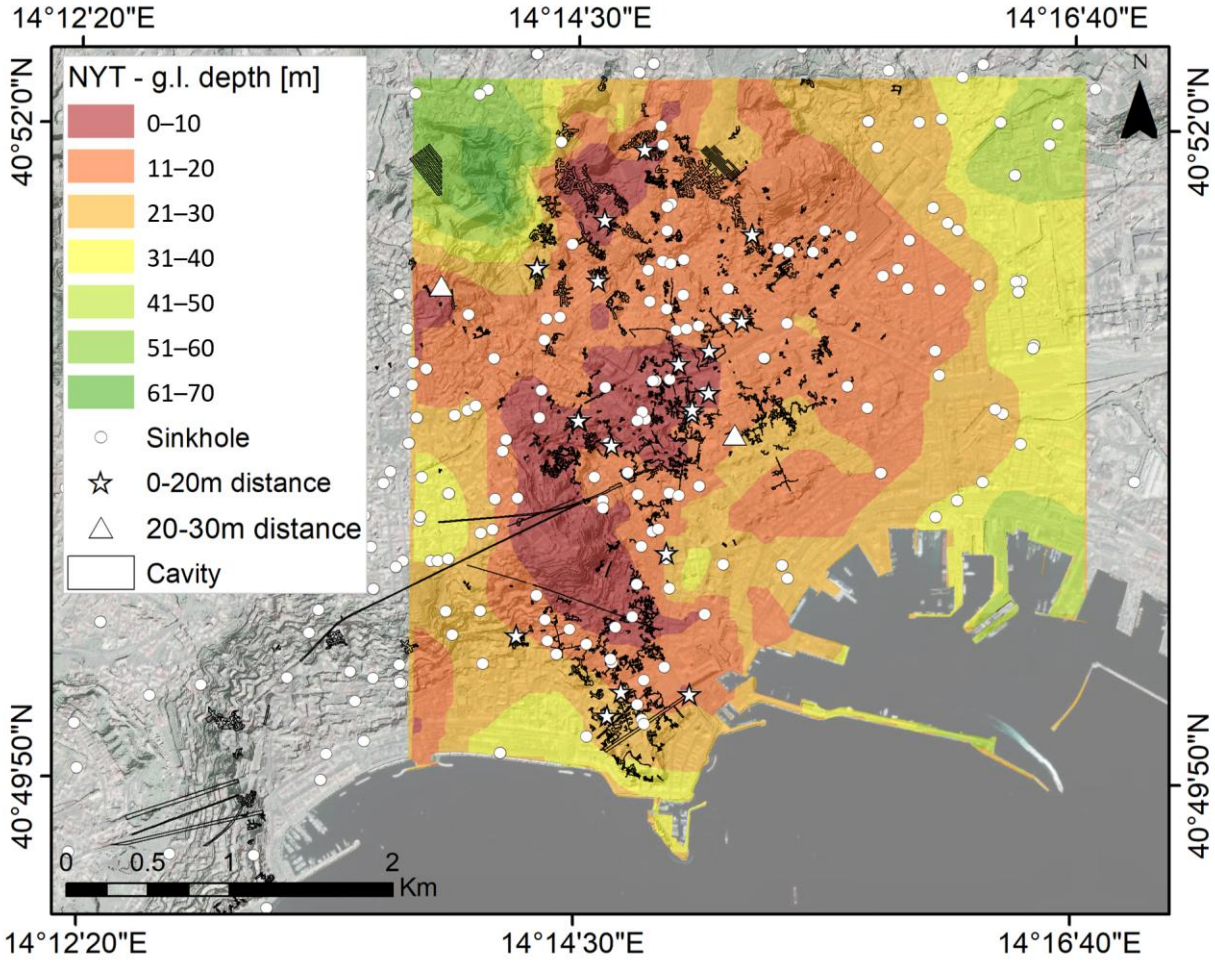


**Figure S7.** Spatial distribution of cavities and sinkholes inventories together with the NYT depth representation from the ground level. Different symbols are used for sinkholes located within 20 m and between 20 m and 30 m from the cavities.